Computer Physics Communications 185 (2014) 1582–1588

Contents lists available at ScienceDirect

Computer Physics Communications

journal homepage: www.elsevier.com/locate/cpc

Higher-order correction to the FDTD method based on the integral form of Maxwell's equations

Naofumi Kitsunezaki *, Atsushi Okabe

Department of Integrated Information Technology, College of Science and Engineering, Aoyama Gakuin University, Sagamihara, Kanagawa, 252-5258, Japan

ARTICLE INFO

Article history:
Received 28 May 2013
Received in revised form
17 February 2014
Accepted 19 February 2014
Available online 28 February 2014

Keywords:
FDTD method
Higher-order correction
The integral form of Maxwell's equations

ABSTRACT

We propose a higher-order correction to the finite-difference time-domain (FDTD) method based on the integral form of Maxwell's equations. We calculate the errors between the numerical and analytic solutions. Numerical solutions are obtained by the original method and our corrected FDTD method to show that the accuracy and reliability of our corrected FDTD method is superior to that of the original FDTD method.

1. Introduction

The finite-difference time-domain (FDTD) method [1] is used in various fields, such as optical analysis for an optical device, including waveguide array, antenna analysis, and so on. In the FDTD method, space and time coordinates of the electric and magnetic fields are discretized into the dual lattice, which is usually called the Yee lattice.

Higher-order correction to the FDTD method in terms of space has been studied [2–11]. In these studies, the approximation is based on the differential form of Maxwell's equations, and the central difference on a cell edge is corrected to coincide with the spatial differential in the corresponding space continuum up to the next lowest-order accuracy of the cell size. In the zero cell-size limit, the central difference on a cell edge in their corrected FDTD method coincides with the corresponding partial differential in the space continuum, and when the cell size is finite, the central difference in the corrected FDTD method is more accurate than that of the original one.

Differential forms of Maxwell's equations are equivalent to the integral forms of these equations after integrating them over the corresponding cell in the space continuum. However, because the algorithm of FDTD method is essentially based on the integral form of Maxwell's equations, the results of previous works [2–11] still have the lowest order of errors because they have not corrected the integral over a cell surface and the edges around the cell.

In this article we discuss the next lowest-order accuracy of Maxwell's equations in the integral form to eliminate the lowest-order error caused by line and surface integrals. We also assume the spatial dimension as 2 for simplicity. However, the application of this higher-order to three spatial dimensions is straightforward. We show some numerical results to prove that the accuracy is improved by our corrected FDTD method.

2. Correction to the FDTD method

In this article, we apply Maxwell's equations in the integral form, especially Faraday's and Ampére–Maxwell's laws, to each cell (Fig. 1). For example, when the cell surface lies on the x–y plane, these laws are written as:

$$\frac{d}{dt}\int_{\blacksquare} dx'dy'\mu H_z\left(t, x+x', y+y', z+\frac{\Delta z}{2}\right) = -\int_{\square} d\mathbf{s}'\cdot\mathbf{E}\left(t, x+x', y+y', z+\frac{\Delta z}{2}\right), \tag{1}$$

$$\frac{d}{dt}\int_{\blacksquare} dx'dy'\varepsilon E_z\left(t, x+x', y+y', z+\frac{\Delta z}{2}\right) = \int_{\square} d\mathbf{s}'\cdot\mathbf{H}\left(t, x+x', y+y', z+\frac{\Delta z}{2}\right) + \int_{\blacksquare} dx'dy' i_z\left(t, x+x', y+y', z+\frac{\Delta z}{2}\right), \tag{2}$$

respectively, where ■ represents the domain $(x', y') \in [-\frac{\Delta x}{2}, \frac{\Delta x}{2}] \times [-\frac{\Delta y}{2}, \frac{\Delta y}{2}]$ and □ represents the boundary of the domain.

* Corresponding author.
E-mail addresses: kitsunezaki@it.aoyama.ac.jp (N. Kitsunezaki), atsushi.okabe@hotmail.co.jp (A. Okabe).

http://dx.doi.org/10.1016/j.cpc.2014.02.022
0010-4655/

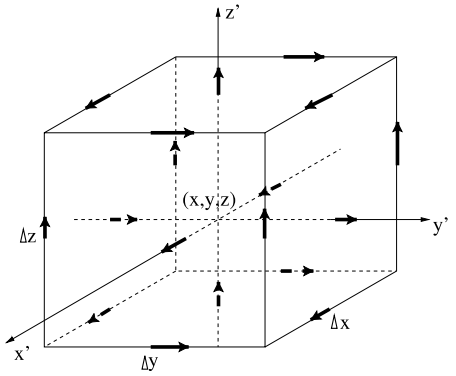

Fig. 1. A cell in the Yee lattice with size $\Delta x \times \Delta y \times \Delta z$. (x, y, z) is the central coordinate of the cell. A parallel component to the edge of the electric field lies at the center of each edge. A vertical component to the surface exists at the center of each surface.

When the center of the cell is described as (x, y, z), the length of each cell edge is $(\Delta x, \Delta y, \Delta z)$, and the time step is Δt, and the next lowest-order approximation of the integral over the cell surface can be written as:

$$\begin{aligned}&\int_{\blacksquare} dx'dy' H_z\left(t, x+x', y+y', z+\frac{\Delta z}{2}\right)\\ &= \left[H_z\left(t, x, y, z+\frac{\Delta z}{2}\right) + \frac{1}{24}\left\{\partial_x^2 H_z\left(t, x, y, z+\frac{\Delta z}{2}\right)\right.\right.\\ &\quad \left.\left.\times\ (\Delta x)^2 + \partial_y^2 H_z\left(t, x, y, z+\frac{\Delta z}{2}\right)(\Delta y)^2\right\}\right]\Delta x\Delta y, \end{aligned} \tag{3}$$

and the same order of approximation of the line integral over one of the cell edges can be written as:

$$\begin{aligned}&\int_{-\frac{\Delta x}{2}}^{\frac{\Delta x}{2}} dx' E_x\left(t, x+x', y-\frac{\Delta y}{2}, z+\Delta z\right)\\ &= \left[E_x\left(t, x, y-\frac{\Delta y}{2}, z+\frac{\Delta z}{2}\right)\right.\\ &\quad \left. + \frac{1}{24}\partial_x^2 E_x\left(t, x, y-\frac{\Delta y}{2}, z+\frac{\Delta z}{2}\right)(\Delta x)^2\right]\Delta x. \end{aligned} \tag{4}$$

Because the second-order derivatives cannot be calculated directly on the Yee lattice, they must be replaced by values defined on it. We apply the following relationship for any function $f(x)$:

$$\partial_x^2 f(x)(\Delta x)^2 = f(x+\Delta x) + f(x-\Delta x) - 2f(x). \tag{5}$$

Then, Eq. (3) becomes:

$$\begin{aligned}&\Phi_z\left(t, x, y, z+\frac{\Delta z}{2}\right)\\ &= \mu\int_{\blacksquare} dx'dy' H_z\left(t, x+x', y+y', z+\frac{\Delta z}{2}\right), \end{aligned} \tag{6}$$

$$\begin{aligned}&= \mu\left[\frac{5}{6}H_z\left(t, x, y, z+\frac{\Delta z}{2}\right)\right.\\ &\quad + \frac{1}{24}\left\{H_z\left(t, x+\Delta x, y, z+\frac{\Delta z}{2}\right)\right.\\ &\quad + H_z\left(t, x-\Delta x, y, z+\frac{\Delta z}{2}\right)\\ &\quad + H_z\left(t, x, y+\Delta y, z+\frac{\Delta z}{2}\right)\\ &\quad \left.\left. + H_z\left(t, x, y-\Delta y, z+\frac{\Delta z}{2}\right)\right\}\right]\Delta x\Delta y, \end{aligned} \tag{7}$$

where Φ_z represents the magnetic flux through the region ■, and Eq. (4) becomes:

$$\begin{aligned}&\int_{\square} d\mathbf{s}'\cdot\mathbf{E}\left(t, x+x', y+y', z+\frac{\Delta z}{2}\right)\\ &= \left[\frac{11}{12}\left\{E_x\left(t, x, y-\frac{\Delta y}{2}, z+\frac{\Delta z}{2}\right)\right.\right.\\ &\quad - E_x\left(t, x, y+\frac{\Delta y}{2}, z+\frac{\Delta z}{2}\right)\Big\}\\ &\quad + \frac{1}{24}\left\{E_x\left(t, x-\Delta x, y-\frac{\Delta y}{2}, z+\frac{\Delta z}{2}\right)\right.\\ &\quad - E_x\left(t, x-\Delta x, y+\frac{\Delta y}{2}, z+\frac{\Delta z}{2}\right)\\ &\quad + E_x\left(t, x+\Delta x, y-\frac{\Delta y}{2}, z+\frac{\Delta z}{2}\right)\\ &\quad \left.\left. - E_x\left(t, x+\Delta x, y+\frac{\Delta y}{2}, z+\frac{\Delta z}{2}\right)\right\}\right]\Delta x - (x\leftrightarrow y), \end{aligned} \tag{8}$$

where $(x \leftrightarrow y)$ means changing x and y in all of the following terms. For example,

$$\begin{aligned}&E_x(t, x, y+\Delta y, z)\Delta x - (x\leftrightarrow y)\\ &= E_x(t, x, y+\Delta y, z)\Delta x - E_y(t, x+\Delta x, y, z)\Delta y. \end{aligned} \tag{9}$$

Differing from the conventional FDTD method, the right-hand side of Eq. (7) is a linear combination of the magnetic field at five different points. From Eqs. (6) and (7), and because H_z is defined on discrete points, such as $(x, y) = (m\Delta x, n\Delta y)$ where m, n are in a finite subset of the integer, a matrix exists representing the linear transformation from H_z to Φ_z, such as

$$\begin{aligned}&\Phi_z\left(t, m\Delta x, n\Delta y, z+\frac{\Delta z}{2}\right)\\ &= \mu\sum_{k,l} S_{xy}(m, n; k, l) H_z\left(t, k\Delta x, l\Delta y, z+\frac{\Delta z}{2}\right), \end{aligned} \tag{10}$$

where $S_{xy}(m, n; k, l)$ is the matrix element of S_{xy} and is defined to satisfy Eq. (7). The symbol S_{xy} is intended to the approximated integral over the cell in the x–y plane. For example, when $(m\Delta x, n\Delta y)$ is neither edge nor corner of the calculation domain,[1]

$$\begin{aligned}S_{xy}(m, n; k, l) = &\left\{\frac{5}{6}\delta_{m,k}\delta_{n,l} + \frac{1}{24}(\delta_{m,k+1}\delta_{n,l} + \delta_{m,k-1}\delta_{n,l}\right.\\ &\left. + \delta_{m,k}\delta_{n,l+1} + \delta_{m,k}\delta_{n,l-1})\right\}\Delta x\Delta y, \end{aligned} \tag{11}$$

where $\delta_{k,l}$ is the Kronecker delta defined as:

$$\delta_{k,l} = \begin{cases}1 & (k = l)\\ 0 & (k \neq l).\end{cases} \tag{12}$$

Then, Faraday's law in the Yee lattice becomes

$$\begin{aligned}&\mu\frac{S_{xy}\left[H_z\left(t+\frac{\Delta t}{2}, x, y, z+\frac{\Delta z}{2}\right) - H_z\left(t-\frac{\Delta t}{2}, x, y, z+\frac{\Delta z}{2}\right)\right]}{\Delta t}\\ &= -(\text{r.h.s. of Eq. (8)}), \end{aligned} \tag{13}$$

where

$$\begin{aligned}&S_{xy}\left(H_z\left(t, x, y, z+\frac{\Delta z}{2}\right)\right)\\ &= \frac{1}{\mu}\sum_{(x', y')} S_{xy}(x, y; x', y') H_z\left(t, x', y', z+\frac{\Delta z}{2}\right). \end{aligned} \tag{14}$$

[1] The matrix elements for $(m\Delta x, n\Delta y)$ representing the edge or corner of the calculation domain is shown in Appendix A.

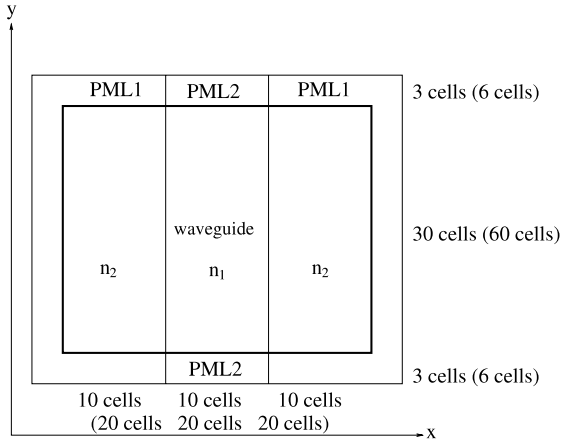

Fig. 2. Design of the calculation domain. The size of the domain is $3.6\lambda \times 3.6\lambda$. For each direction, the domain is divided into 36×36 or 72×72 cells.

Hence, all values of H_z on the Yee lattice at time $t + \frac{\Delta t}{2}$ are derived from that at time $t - \frac{\Delta t}{2}$, and all values of E_x and E_y on the Yee lattice at time t as

$$H_z\left(t + \frac{\Delta t}{2}, x, y, z + \frac{\Delta z}{2}\right) = H_z\left(t - \frac{\Delta t}{2}, x, y, z + \frac{\Delta z}{2}\right) + \frac{\Delta t}{\mu} S_{xy}^{-1} \quad \text{(r.h.s. of Eq. (8))}, \tag{15}$$

where

$$\sum_{x'',y''} S_{xy}(x, y; x'', y'') S_{xy}^{-1}(x'', y''; x', y') = \delta_{x,x'}\delta_{y,y'}. \tag{16}$$

Other components H_x, H_y are also derived in a similar way.

In a similar way, Ampére–Maxwell's law is also modified to

$$E_z\left(t + \frac{\Delta t}{2}, x, y, z + \frac{\Delta z}{2}\right) = E_z\left(t - \frac{\Delta t}{2}, x, y, z + \frac{\Delta z}{2}\right) - \frac{\Delta t}{\varepsilon} i_z\left(t, x, y, z + \frac{\Delta z}{2}\right) + \frac{\Delta t}{\varepsilon} S_{xy}^{-1} \quad \text{(r.h.s. of Eq. (8) with } E \text{ replaced by } H\text{)}. \tag{17}$$

Other components E_x, E_y are also derived in a similar way.

The stability criterion is obtained as:

$$c_{\max}\Delta t \le \frac{2}{3} \frac{1}{\sqrt{\left(\frac{1}{\Delta x}\right)^2 + \left(\frac{1}{\Delta y}\right)^2 + \left(\frac{1}{\Delta z}\right)^2}}, \tag{18}$$

where $c_{\max}$ is the maximum wave velocity expected within the model. The derivation of Eq. (18) is shown in Appendix B. The upper limit of the time step in our corrected FDTD method is shorter than the original one to achieve higher accuracy for a given spatial resolution.

3. Numerical results

To compare the accuracy and reliability of the original and our corrected FDTD methods, we have numerically calculated the amplitude of the magnetic field propagating a system including a waveguide, to obtain

$$err(t) = \frac{\sum_{j_x, j_y} \{H_z^{\text{num}}(t, j_x\Delta x, j_y\Delta y) - H_z^{\text{anl}}(t, j_x\Delta x, j_y\Delta y)\}^2}{\sum_{j_x, j_y} H_z^{\text{anl}}(t, j_x\Delta x, j_y\Delta y)^2}, \tag{19}$$

where $H_z^{\text{num}}(t, j_x\Delta x, j_y\Delta y)$ indicates the result of the numerically calculated magnetic field and $H_z^{\text{anl}}(t, j_x\Delta x, j_y\Delta y)$ indicates the result of the analytically calculated one for infinitely long x- and y-directions.

As shown in Fig. 2, the calculation domain has $3.6\lambda \times 3.6\lambda$ size and is divided into 36×36 or 72×72 cells, where λ is the wavelength of the plane wave. In each cell, the x component of the magnetic field is configured at the center of the cell, and the parallel component of the electric field to the edge lies at the center of each edge of the cell. A waveguide lies in the center of the calculation domain. The width of the waveguide is λ and its refractive index is n_1. The other region has refractive index n_2. On the border of the refractive indexes, we use a layer of cells with refractive index $\sqrt{(n_1^2 + n_2^2)/2}$. We use the same calculation algorithm on and around the border with the other region except for the edge and corner of the calculation domain. The time step converted to spatial dimension $c_0\Delta t$ is $1.0 \times 10^{-3}\lambda$, where c_0 is the speed of light in vacuum. In our calculation, $\Delta x = \Delta y = 0.1\lambda$ or 0.05λ, so that the r.h.s. in Eq. (19) is $4.7 \times 10^{-2}\lambda$ or $2.4 \times 10^{-2}\lambda$. Therefore, the l.h.s. of Eq. (19) is much smaller than r.h.s, so any numerical error caused by finiteness of the time step is negligible. The perfect matching layer (PML) is used to absorb the energies of the electric and magnetic fields so that no wave is reflected by the PMLs [12]. In the calculation domain, we have two types of regions with different refractive indexes. Thus, we used two types of PML so that the refractive index of the PML is the same as the bordering analytic region. In our calculations, the width of PML is three cells (0.3 lambda), so that the analytic domain, which is the domain surrounded in the bold line in Fig. 2, has $3\lambda \times 3\lambda$ area. The effectiveness of the PML used is discussed in Appendix C. We excite the wave just above the bottom PML to generate the wave propagating in the y-direction. Such a magnetic field, whose coordinate in the y-axis is y_0, is excited as

$$H_z(t, x, y_0) = H_0(x)\sin(\omega t), \tag{20}$$

$$H_0(x) = \begin{cases} h_0 \cos\left(\dfrac{2Px}{\lambda}\right) & |x| \le \dfrac{\lambda}{2} \\ h_0 \cos(P) e^{-\frac{Q(2|x|-\lambda)}{\lambda}} & \dfrac{\lambda}{2} \le |x| \end{cases} \tag{21}$$

where P and Q satisfy

$$Q = \left(\frac{n_2}{n_1}\right)^2 P\tan(P), \tag{22}$$

$$P^2 + Q^2 = \pi^2(n_1^2 - n_2^2). \tag{23}$$

The square root of the r.h.s. in Eq. (23) is called the V-parameter.

One important dimensionless parameter $\beta\lambda$, which is the product of the propagation constant and the wavelength, is given using the solution of Eqs. (22) and (23) as

$$\beta\lambda = \frac{2\pi\sqrt{n_1^2Q^2 + n_2^2P^2}}{V}. \tag{24}$$

Eq. (21) is an analytic solution in the x-direction for the waveguide system shown in Fig. 2, where the x- and y-directions are infinitely extended. In this system, non-zero components of the electric and magnetic fields are H_z, E_x, and E_y.

In Eq. (19), we use H_z to evaluate the error between numerical and analytical calculations because the y dependence of the analytic solution can be easily obtained by replacing ωt with $\omega t - \beta(y - y_0)$ in Eq. (20).

Fig. 3 shows the $err(t)$ functions for $(n_1, n_2) = (1.50, 1.49)$. In this case, parameters P, Q, V, and $\beta\lambda$ are:

$$P = 0.48257, \tag{25}$$
$$Q = 0.24945, \tag{26}$$
$$V = 0.54323, \tag{27}$$
$$\beta\lambda = 9.3752. \tag{28}$$

Because $0 < V < \frac{\pi}{2}$, this is single-mode waveguide system.

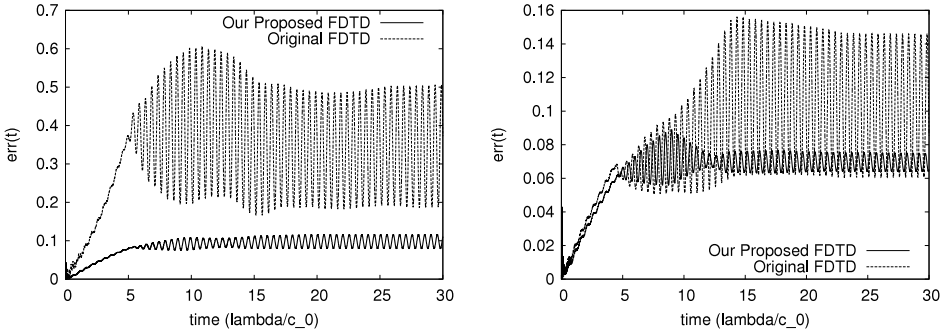

(a) Cell size is 0.1λ. (b) Cell size is 0.05λ.

Fig. 3. Values of $err(t)$ of the eigenmode in a waveguide system for the original FDTD method and our corrected FDTD method when $(n_1, n_2) = (1.50, 1.49)$.

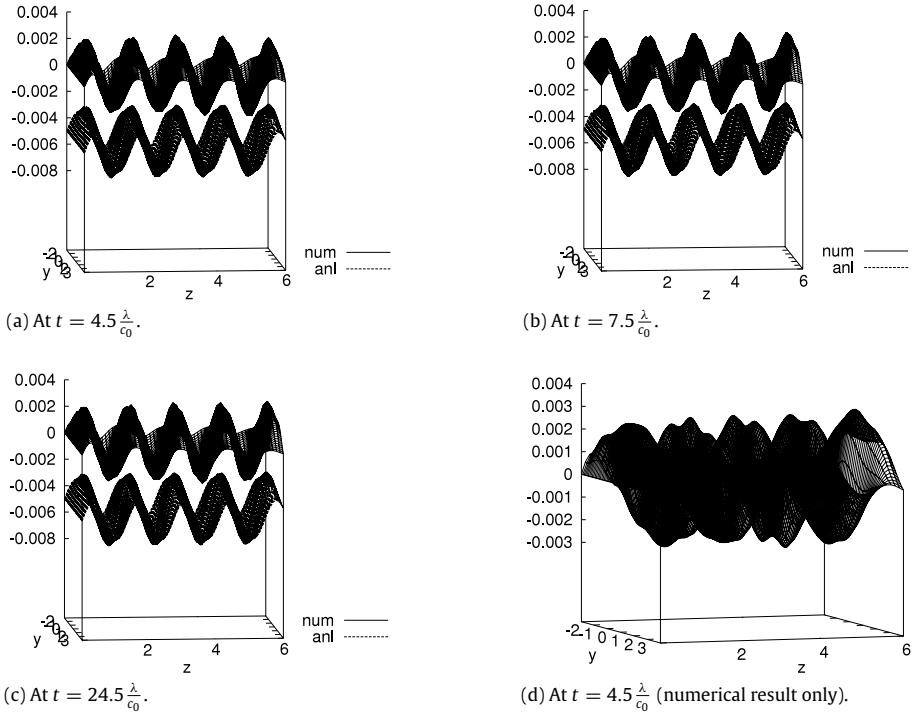

(a) At $t = 4.5\frac{\lambda}{c_0}$. (b) At $t = 7.5\frac{\lambda}{c_0}$.

(c) At $t = 24.5\frac{\lambda}{c_0}$. (d) At $t = 4.5\frac{\lambda}{c_0}$ (numerical result only).

Fig. 4. Numerical (top) and analytic (bottom) results of the magnetic field amplitude. The numerical result is calculated using our corrected FDTD method and the cell size is 0.05λ.

In Fig. 3, $H_z(0, j_x\Delta x, j_y\Delta y) = 0$ at $t = 0$ for any j_x and j_y, and $H_z(t, j_x\Delta x, 0)$ for each j_x is excited as Eq. (20). The first wave-front in the cladding region whose index is n_2 reaches the top border of the analytic region at $t = 4.47\frac{\lambda}{c_0}$. The first wave-front in the core region whose index is n_1 reaches the top border at $t = 4.5\frac{\lambda}{c_0}$. Fig. 4 shows the calculation results of the magnetic field amplitude at $t = 4.5\frac{\lambda}{c_0}$ using our corrected FDTD method with the size 0.05λ. The calculation results become quasi-stable after $t = 4.5\frac{\lambda}{c_0}$. Fig. 4(b) and (c) show the calculation results of the magnetic field amplitude at $t = 7.5\frac{\lambda}{c_0}$ and $t = 24.5\frac{\lambda}{c_0}$, respectively. Although Fig. 3(b) shows that the errors between $t = 5\frac{\lambda}{c_0}$ and $t = 13\frac{\lambda}{c_0}$ and those after $t = 15\frac{\lambda}{c_0}$ are different, their difference is not as clear as in Fig. 4(b) and (c).

Comparing the values of the quasi-stable region in Fig. 3(a) and (b), errors of our corrected FDTD method seem to be saturated. Fig. 4(d) shows the numerical result using our corrected FDTD method at $t = 24.5\frac{\lambda}{c_0}$ with 0.05λ cell size. As shown in the figure, envelopes in the x-direction at all peaks in the y-direction are different. Although they are symmetric in the x-direction, the first (left) and last (right) peaks have one peak, the third and fourth peaks have two peaks, and the second peak has three peaks. Such phenomena are observed in our corrected FDTD method with 0.1λ cell size and the original FDTD method with 0.1λ and 0.05λ cell sizes. Since the system is a single-mode waveguide, it seems that some of the incident wave transit to radiation modes that are irrelevant to the waveguide system.

The reason for such a mode transition is thought to be that our system is too short to be regarded as a waveguide. In a waveguide system, only certain light rays with a particular incident angle to the border of reflective indexes in the core region survive and propagate, because of phase matching between parallel light-rays in the core region [13]. Such phase mismatching occurs when the length of the waveguide is infinite. In contrast, the waveguide in our system is only 3λ, so short that irrelevant light-rays not of the particular incident angle in the core region survive to generate other modes than the originally generated propagation mode.

In Fig. 3, the solid line shows $err(t)$ function of our corrected FDTD method and the dotted line is that of the original FDTD

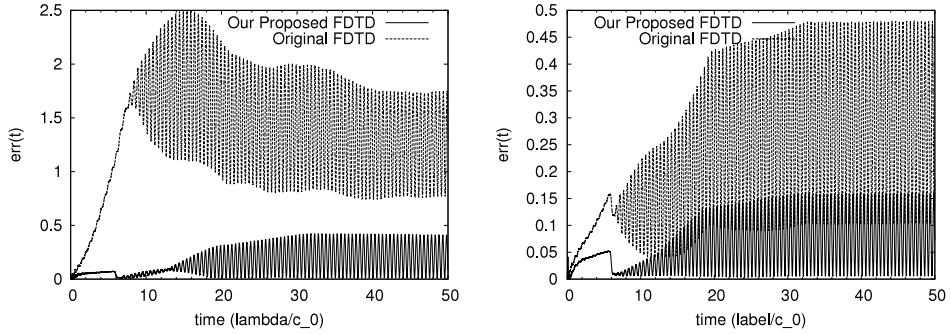

(a) Cell size is 0.1λ. (b) Cell size is 0.05λ.

Fig. 5. Result for waves propagating on waveguide with $(n_1, n_2) = (2.0, 1.0)$.

method. Fig. 3 shows the $err(t)$ functions when the cell size is $\lambda/10$. It shows that the $err(t)$ function of our corrected FDTD method is always less than that of original FDTD method. This result indicates that our corrected FDTD method is more accurate and reliable than the original FDTD method. Fig. 3(b) shows that when cell size is $\lambda/20$ as shown in the figure, the upper envelope of $err(t)$ function of our corrected FDTD method is less than that of original FDTD method, again indicating that our corrected FDTD method is more reliable than the original FDTD method.

Fig. 5 shows the result for $err(t)$ functions of our corrected FDTD method and the original FDTD method when $(n_1, n_2) = (2.0, 1.0)$. As shown in Fig. 3, the solid line shows $err(t)$ function of our corrected FDTD method, and the dotted line shows that of the original FDTD method. In this case, parameter V is:

$$V = 5.4414. \tag{29}$$

Because $V > \frac{\pi}{4}$, this is a multimode waveguide system. In the mode having largest propagation constant, parameters P, Q, and $\beta\lambda$ are

$$P = 1.4993, \tag{30}$$

$$Q = 5.2308, \tag{31}$$

$$\beta\lambda = 12.203. \tag{32}$$

In Fig. 5, $H_z(0, j_x\Delta x, j_y\Delta y) = 0$ at $t = 0$ for any j_x and j_y, and $H_z(t, j_x\Delta x, 0)$ for each j_x is excited as Eq. (20). The first wave-front in the cladding region reaches the top border at $t = 3\frac{\lambda}{c_0}$. The first wave-front in the core region reaches the top border at $t = 6\frac{\lambda}{c_0}$. The system becomes quasi-stable after $t = 6\frac{\lambda}{c_0}$.

Fig. 5(a) shows the $err(t)$ functions when the cell size is $\lambda/10$. Similar to Fig. 3(b), $err(t)$ function of our corrected FDTD method is always less than that of the original FDTD method. This result supports that our corrected FDTD method is more accurate and reliable than the original FDTD method. Fig. 5(b) shows $err(t)$ functions when the cell size is $\lambda/20$. Although regions exist in which the maximal value of $err(t)$ of our corrected FDTD method is larger than the minimal value of that of the original FDTD method, the upper envelope of $err(t)$ function of our corrected FDTD method is less than that of the original FDTD method, as the result shows in Fig. 3(b). This result supports our corrected FDTD method and is more reliable than the original FDTD method.

4. Conclusion and discussion

In this article, we propose a novel approach for improving the accuracy of the FDTD method by correcting the accuracy of the integral form of Maxwell's equations, especially for Faraday's and Ampére–Maxwell's laws. We also show that errors between numerical and analytic solutions using the $err(t)$ function defined in Eq. (19). Our results indicates that the larger the cell size becomes, the larger the difference between $err(t)$ functions of our corrected and original FDTD methods, where in a suitable range which is larger than the period of fluctuation of $err(t)$ functions, the mean values of our corrected and original FDTD methods are less than those of the original FDTD methods. This means that the larger the cell size, the more reliable our corrected FDTD method is in comparison with the original one, and if the size is sufficiently large, our corrected FDTD method is always the more accurate.

On the other hand, when the cell size is small, errors of our corrected FDTD method seems to not improve as expected. In all numerical results using our corrected FDTD method and original FDTD method, we observed similar phenomena in which the envelopes in the x-direction of the propagating wave at every peaks in the y-direction have different forms from originally generated one, which is the eigenfunction of the waveguide system. This fact suggests that the analytic solution of waveguide system do not agree with the exact solution for the system represented by Fig. 2, because it does not have infinite length. We should consider a longer waveguide (10λ or more), or alternatively remove irrelevant modes that would not exist if the waveguide were to have infinite length.

For any calculation that uses the FDTD method, each cell has a finite area. Moreover, Maxwell's equations in the integral form are exact and well-defined for any surface having a finite area. On the other hand, Maxwell's equations in differential forms are only well defined in zero size limit, and they are ill-defined on finite area. For example, we can insist that physical parameters such as dielectric permittivity or magnetic permeability may depend on cell size such as in lattice quantum electrodynamics or lattice quantum chromodynamics [14]. Because of these facts, it is natural that the algorithm of FDTD method should be based on integral form of Maxwell's equations.

Acknowledgments

The authors would like to thank all the members of the Mizusawa Laboratory in the Department of Integrated Information Technology, College of Science and Engineering, Aoyama Gakuin University, Japan, for their valuable discussions and comments. The authors would also like to thank NIPPON THERMONICS. Co., Ltd. for financial support of our research.

Appendix A. Surface integral over a cell at the edge and corner

As shown in Eqs. (6) and (7), and because (x, y) is defined at the center of the integral domain, the r.h.s. of Eq. (6) is equal to Eq. (7) to the fifth order of Δx and Δy. When (x, y) represents a center of a corner or an edge cell in the analytic domain, Eq. (7) is invalid because there is at least one direction in which no adjacent cell exists.

When (x, y) is at the bottom-left corner of the analytic domain, Eqs. (6) and (3) are replaced as:

$$\begin{aligned}
&\Phi_z\left(t, x, y, z+\frac{\Delta z}{2}\right)\\
&\quad=\mu\left\{\frac{7}{6}H_z\left(t, x, y, z+\frac{\Delta z}{2}\right)\right.\\
&\qquad-\frac{5}{24}H_z\left(t, x+\Delta x, y, z+\frac{\Delta z}{2}\right)\\
&\qquad+\frac{1}{6}H_z\left(t, x+2\Delta x, y, z+\frac{\Delta z}{2}\right)\\
&\qquad-\frac{1}{24}H_z\left(t, x+3\Delta x, y, z+\frac{\Delta z}{2}\right)\\
&\qquad-\frac{5}{24}H_z\left(t, x, y+\Delta y, z+\frac{\Delta z}{2}\right)\\
&\qquad+\frac{1}{6}H_z\left(t, x, y+2\Delta y, z+\frac{\Delta z}{2}\right)\\
&\qquad\left.-\frac{1}{24}H_z\left(t, x, y+3\Delta y, z+\frac{\Delta z}{2}\right)\right\},
\end{aligned}\tag{A.1}$$

to have the same order of accuracy with Eq. (3). The integrals over the other corner cells are also defined similarly as in Eq. (A.1).

When (x, y) is at the bottom but not the corner of the analytic domain, Eqs. (6) and (3) are replaced as:

$$\begin{aligned}
&\Phi_z\left(t, x, y, z+\frac{\Delta z}{2}\right)\\
&\quad=\mu\left[H_z\left(t, x, y, z+\frac{\Delta z}{2}\right)\right.\\
&\qquad+\frac{1}{24}\left\{H_z\left(t, x-\Delta x, y, z+\frac{\Delta z}{2}\right)\right.\\
&\qquad\left.+H_z\left(t, x+\Delta x, y, z+\frac{\Delta z}{2}\right)\right\}\\
&\qquad-\frac{5}{24}H_z\left(t, x, y-\Delta y, z+\frac{\Delta z}{2}\right)\\
&\qquad+\frac{1}{6}H_z\left(t, x, y-2\Delta y, z+\frac{\Delta z}{2}\right)\\
&\qquad\left.-\frac{1}{24}H_z\left(t, x, y-3\Delta y, z+\frac{\Delta z}{2}\right)\right].
\end{aligned}\tag{A.2}$$

The integrals over the other edges, but not the corner, are also defined similarly as in Eq. (A.2), so that the r.h.s. of Eq. (A.2) has the same accuracy as in Eq. (3).

Appendix B. Derivation of the stability criterion

Our derivation of the stability criterion is based on the argument in Ref. [15]. To derive it, a complex vector $\mathbf{V}$ is defined as

$$\mathbf{V}=Z_0\mathbf{H}+i\mathbf{E},\tag{B.1}$$

where $Z_0=\sqrt{\frac{\mu}{\varepsilon}}$. $\mathbf{V}$ satisfies the following differential equation:

$$\frac{1}{c}\partial_t\mathbf{V}=i\nabla\times\mathbf{V},\tag{B.2}$$

because of Maxwell's equations in differential form. Because the l.h.s. of Eq. (B.2) only includes time derivative and the r.h.s. of that only includes space derivative, the separation of variables can be applied to $\mathbf{V}$, and a scalar κ exists such that

$$\frac{1}{c}\partial_t\mathbf{V}=\kappa\mathbf{V},\tag{B.3}$$

$$i\nabla\times\mathbf{V}=\kappa\mathbf{V}.\tag{B.4}$$

Because our correction does not modify the time direction algorithm, κ for any k_x, k_y, and k_z is restricted to the region

$$\mathrm{Re}\,\kappa=0,\qquad|\mathrm{Im}\,\kappa|\le\frac{2}{c\Delta t},\tag{B.5}$$

because of the stability condition [15].

When both sides of Eq. (B.4) are integrated over a cell surface in x–y plane, and applied the next lowest-order approximation over the cell edge for the l.h.s. in Eq. (8) and over the cell surface for the r.h.s. in Eq. (7), Eq. (B.4) is modified to

$$\begin{aligned}
&i\left[\frac{11}{12}\left\{V_x\left(t, x, y-\frac{\Delta y}{2}, z\right)-V_x\left(t, x, y+\frac{\Delta y}{2}, z\right)\right\}\right.\\
&\qquad+\frac{1}{24}\left\{V_x\left(x-\Delta x, y-\frac{\Delta y}{2}, z\right)\right.\\
&\qquad-V_x\left(x-\Delta x, y+\frac{\Delta y}{2}, z\right)+V_x\left(x+\Delta x, y-\frac{\Delta y}{2}, z\right)\\
&\qquad\left.\left.-V_x\left(x+\Delta x, y+\frac{\Delta y}{2}, z\right)\right\}\right]\Delta x-(x\leftrightarrow y)\\
&\quad=\left[\frac{5}{6}V_z(t, x, y, z)+\frac{1}{24}\{V_z(t, x-\Delta x, y, z)\right.\\
&\qquad+V_z(t, x+\Delta x, y, z)+V_z(t, x, y+\Delta y, z)\\
&\qquad\left.+V_z(t, x, y-\Delta y, z)\}\right]\Delta x\Delta y.
\end{aligned}\tag{B.6}$$

As in Ref. [15], we now let

$$\mathbf{V}(t, x, y, z)=\mathbf{V_0}(t)e^{i(k_xx+k_yy+k_zz)},\tag{B.7}$$

then, Eq. (B.6) becomes

$$\begin{aligned}
&\frac{1}{6}e^{i(k_xx+k_yy+k_zz)}\left[\{11+\cos(k_x\Delta x)\}\sin\left(\frac{k_y\Delta y}{2}\right)(V_0)_x(t)\Delta x\right.\\
&\qquad\left.-\{11+\cos(k_y\Delta y)\}\sin\left(\frac{k_x\Delta x}{2}\right)(V_0)_y(t)\Delta y\right]\\
&\quad=\kappa\frac{1}{6}e^{i(k_xx+k_yy+k_zz)}\left[5+\frac{1}{2}\{\cos(k_x\Delta x)+\cos(k_y\Delta y)\}\right]\\
&\qquad\times(V_0)_z(t)\Delta x\Delta y.
\end{aligned}\tag{B.8}$$

When a cell surface is in y–z and x–z plane, similar equations as Eq. (B.8) can be derived, and combining these equations, the following equation is derived:

$$\begin{aligned}
&\begin{pmatrix}
0 & B_y\dfrac{\sin\left(\frac{k_z\Delta z}{2}\right)}{\Delta z} & -B_z\dfrac{\sin\left(\frac{k_y\Delta y}{2}\right)}{\Delta y}\\
-B_x\dfrac{\sin\left(\frac{k_z\Delta z}{2}\right)}{\Delta z} & 0 & B_z\dfrac{\sin\left(\frac{k_x\Delta x}{2}\right)}{\Delta x}\\
B_x\dfrac{\sin\left(\frac{k_y\Delta y}{2}\right)}{\Delta y} & -B_y\dfrac{\sin\left(\frac{k_x\Delta x}{2}\right)}{\Delta x} & 0
\end{pmatrix}\begin{pmatrix}(V_0)_x\\(V_0)_y\\(V_0)_z\end{pmatrix}\\
&\quad=\kappa\begin{pmatrix}A_{yz}(V_0)_x\\A_{zx}(V_0)_y\\A_{xy}(V_0)_z\end{pmatrix},
\end{aligned}\tag{B.9}$$

where

$$A_{yz} = 5 + \frac{\cos(k_y \Delta y) + \cos(k_z \Delta z)}{2}, \tag{B.10}$$
$$B_x = 11 + \cos(k_x \Delta x),$$

$$A_{zx} = 5 + \frac{\cos(k_z \Delta z) + \cos(k_x \Delta x)}{2}, \tag{B.11}$$
$$B_y = 11 + \cos(k_y \Delta y),$$

$$A_{xy} = 5 + \frac{\cos(k_x \Delta x) + \cos(k_y \Delta y)}{2}, \tag{B.12}$$
$$B_z = 11 + \cos(k_z \Delta z).$$

Eq. (B.9) has a non-trivial solution iff

$$\kappa = \pm i \left[\frac{B_z B_y}{A_{zx} A_{xy}} \left(\frac{\sin\left(\frac{k_x \Delta x}{2}\right)}{\Delta x} \right)^2 + \frac{B_x B_z}{A_{xy} A_{yz}} \left(\frac{\sin\left(\frac{k_y \Delta y}{2}\right)}{\Delta y} \right)^2 + \frac{B_y B_x}{A_{yz} A_{zx}} \left(\frac{\sin\left(\frac{k_z \Delta z}{2}\right)}{\Delta z} \right)^2 \right]^{\frac{1}{2}}. \tag{B.13}$$

Combining Eq. (B.13) with Eq. (B.5), and using the arbitrary property of k_x, k_y, and k_z,

$$\sup_{\{k_x, k_y, k_z\}} |Im\, \kappa| = 3 \left[\left(\frac{1}{\Delta x}\right)^2 + \left(\frac{1}{\Delta y}\right)^2 + \left(\frac{1}{\Delta z}\right)^2 \right]^{\frac{1}{2}} \leq \frac{2}{c \Delta t}, \tag{B.14}$$

where $\sup_{\{k_x, k_y, k_z\}} |Im\, \kappa|$ means the supremum of the absoluted value of κ for any k_x, k_y, and k_z. Eq. (18) is directly derived from Eq. (B.14).

Appendix C. The effectiveness of the PML

At least, the PML on the left and right-hand sides in Fig. 2 or other absorbing boundaries are necessary when Q in Eq. (21) is small. For example, when $(n_1, n_2) = (1.50, 1.49)$ as shown in Fig. 3, P and Q are shown in Eqs. (25) and (26), and $H_0(x)$ at the border of the analytic region is $0.53786 \times h_0$. In such a case, the effect of reflection on the border cannot be ignored.

On the other hand, the top PML in Fig. 2 can be removed if we stop the calculation before the electro-magnetic wave reaches the top border of the analytic region. In addition, when we put the magnetic wave sources in one-third bottom of the analytic region, the bottom PML can also be removed, because at least a part of wave going downward reflects at the bottom of the analytic region returns to the wave source when wave going upward reaches the top border (Fig. C.6). In this case the result in the bottom one-third region must be ignored because waves propagating upward and downward are mixed in the region.

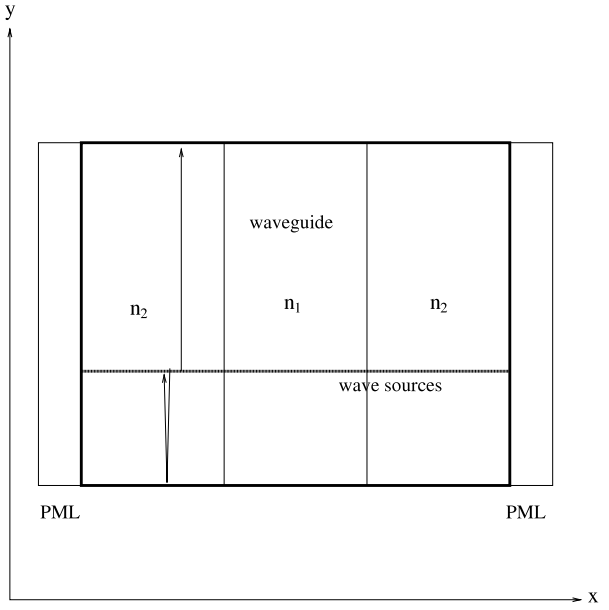

Fig. C.6. Design of the system when the top and bottom PMLs are removed.

References

[1] K.S. Yee, Numerical solution of initial boundary value problems involving Maxwell's equations in isotropic media, IEEE Trans. Antennas Propag. AP-14 (1966) 302.
[2] S.H. Crandall, Numerical treatment of a fourth order parabolic partial differential equation, JACM 1 (1954) 111.
[3] S.D. Conte, A stable implicit finite difference approximation to a fourth order parabolic equation, J. ACM 4 (1957) 18.
[4] E. Turkel, High-order methods, in: A. Taflove (Ed.), Advances in Computational Electrodynamics: The Finite-Difference Time-Domain Method, Artec House, Norwood, MA, 1988.
[5] K. Lan, Y. Liu, W. Lin, A higher order (2, 4) scheme for reducing dispersion in FDTD algorithm, IEEE Trans. Electromagn. Compat. 41 (1999) 160.
[6] E. Turkel, A. Yefet, On the construction of a high order difference scheme for complex domains in a Cartesian grid, Appl. Numer. Math. 33 (2000) 113.
[7] N.V. Kantartzis, T.D. Tsiboukis, A generalized methodology based on higher-order conventional and non-standard FDTD concepts for the systematic development of enhanced dispersionless wide-angle absorbing perfectly matched layers, Int. J. Numer. Model. 13 (2000) 417.
[8] A. Yefet, E. Turkel, A high order difference scheme for complex domains in a Cartesian grid, Appl. Numer. Math. 33 (2000) 125.
[9] N.V. Kantartzis, T.D. Tsiboukis, Higher-Order FDTD Schemes for Waveguide and Antenna Structures, Morgan and Claypool, San Rafael, CA, 2006.
[10] Z. Xie, C. Chan, B. Zhang, An explicit fourth-order staggered finite-difference time-domain method for Maxwell's equations, J. Comput. Appl. Math. 147 (2002) 75.
[11] Z. Xie, C. Chan, B. Zhang, An explicit fourth-order orthogonal staggered-grid FDTD method for Maxwell's equations, J. Comput. Phys. 175 (2002) 739.
[12] E. Turkel, A. Yefet, Absorbing PML boundary layers for wave-like equations, Appl. Numer. Math. 27 (1998) 533.
[13] K. Okamoto, Fundamentals of Optical Waveguides, Academic Press, San Diego, 2006.
[14] L.P. Kadanoff, Scaling laws for ising models near Tc, Physics 2 (1966) 263; K.G. Wilson, J. Kogut, The renormalization group and the ϵ expansion, Phys. Rep. 12 (1974) 75.
[15] A. Taflove, M.E. Brodwin, Numerical solution of steady-state electromagnetic scattering problems using the time-dependent Maxwell's equations, IEEE Trans. Microw. Theory Tech. MTT-23 (1975) 623.